



HAL
open science

Effects of axial rectangular groove on turbulent Taylor-Couette flow from analysis of experimental data

K. Sadjavi, Florent Ravelet, F. Bakir

► **To cite this version:**

K. Sadjavi, Florent Ravelet, F. Bakir. Effects of axial rectangular groove on turbulent Taylor-Couette flow from analysis of experimental data. 2017. hal-01611013v1

HAL Id: hal-01611013

<https://hal.science/hal-01611013v1>

Preprint submitted on 5 Oct 2017 (v1), last revised 26 Feb 2018 (v2)

HAL is a multi-disciplinary open access archive for the deposit and dissemination of scientific research documents, whether they are published or not. The documents may come from teaching and research institutions in France or abroad, or from public or private research centers.

L'archive ouverte pluridisciplinaire **HAL**, est destinée au dépôt et à la diffusion de documents scientifiques de niveau recherche, publiés ou non, émanant des établissements d'enseignement et de recherche français ou étrangers, des laboratoires publics ou privés.

Effects of axial rectangular groove on turbulent Taylor-Couette flow from analysis of experimental data

K. Sodjavi^a, F. Ravelet^{a,*}, F. Bakir^a

^a*Arts et Metiers ParisTech, DynFluid, 151 boulevard de l'Hôpital, 75013 Paris, France*

Abstract

The relationship between a rough or structured surface topology and its hydraulic resistance was analysed in the case of fully turbulent Taylor-Couette flow at fixed radii ratio $\eta = 0.9375$ and for Reynolds numbers Re_i from 2×10^4 to 13×10^4 . Three configurations of inner cylinder having 6, 12 and 24 grooves of a same rectangular shape and regularly distributed were compared to a reference smooth cylinder with only inner cylinder rotating. Such configurations are common in electric motors of high power density where a better understanding of flow pattern and heat transfer is essential to enhance their design and to develop appropriate cooling system. Torque and pointwise velocity measurements were performed. The effects of the flow modulations induced by the grooves on the friction coefficient and the flow features were examined. The results showed significant difference in the flow pattern and an increase of the friction coefficient with increasing the groove number. However, the drag-increasing capacity of each groove was further reduced by increasing the groove number. It was also found that, the local scaling exponent between friction coefficient and Reynolds number was insensitive to the present surface roughness, suggesting that the bulk flow contribution is similar for all the four configurations.

Keywords: Rough boundary, Rectangular groove, Friction coefficient, Taylor-Couette flow, LDV measurement,

1. Introduction

Fluid flow around solid body of rough or structured surface topology has attracted considerable interest since it is encountered in many natural phenomena and engineering applications. The design of smaller and compact electric motor with high power density is one of the related application. For the latter, the solid body is usually two coaxial cylinders with only inner cylinder rotating. Generally, this configuration is analogous to a canonical topology known as Taylor-Couette flow. For such rotating machinery, the aerodynamic losses in the annulus between the two cylinders are a major issue. Better understanding of the flow field and heat transfer characteristics in this confined environment, however acquired for smooth inner cylinder, still required for rough or axially grooved inner cylinder. This is needed in order to enhance their design and to develop appropriate cooling system. As far as heat and aerodynamic behavior are concerned only a few investigations contain references to an axially grooved cylinder. Likewise, most of the reported results concern global physical quantities.

Among the few studies addressing this issue, we mention Hayase *et al.* [1], who used numerical simulation to compare three different flow configurations in term of velocity and heat transfer coefficient. The authors specifi-

cally studied the influence of twelve cavities embedded in either the inner rotating or the outer fixed cylinder in laminar flow. They observed larger effects, both on the flow and heat transfer when the cavities were located on the inner cylinder rather than on the outer cylinder. Lee and Minkowycz [2] investigated experimentally heat transfer and pressure drop characteristics of four different configurations of only one cylinder rotating and, for Reynolds number Re_i up to 10^3 . The surfaces of the cylinders constituting the annulus were either smooth or one smooth and the other grooved axially. As the previous authors, they noted that the presence of grooves on the rotating inner cylinder significantly increased the heat coefficient, over the smooth cylinder. It was also found that the heat coefficient expressed in term of Nusselt number for all studied configurations having grooves appear to follow a simple correlation at high Taylor number. By the need of additional information on the design of cooling systems for electric motors of high power density, Gardiner and Sabersky [3] measured experimentally heat and pressure drop coefficient of two configurations of coaxial cylinders for axial Reynolds number up to 7×10^3 . A configuration of both smooth cylinders was compared to that of inner grooved cylinder and outer smooth cylinder. As the previous studies, the authors observed an increase of heat coefficient by the grooved cylinder. They also noted that the grooved rotor were associated to friction factors which were generally higher than those for the smooth rotor, but

*Corresponding author

Email address: florent.ravelet@ensta.org (F. Ravelet)

with profiles exhibiting the same trends. As far as the heat transfer between concentric rotating cylinders with non-smooth cylindrical gaps is concerned, the reader should refer to the recent review of Fenot *et al.* [4].

A flow over ribs is one of the well-documented configurations close to those of the above studies. The common ribs are generally square or triangular in shape, and are regularly distributed on either the inner or the outer cylinder surface or on both cylinder surfaces simultaneously. Several experimental studies, such as, for example Cadot *et al.* [5], van den Berg *et al.* [6], Motozawa *et al.* [7] were devoted to the dissipation characterization for Reynolds number up to 30×10^4 . The main conclusions in [5, 6] is that, with two rough cylinders, the drag coefficient was found to be independent of the Reynolds number. The authors observed that, from smooth to ribbed cylinders, the total dissipation was found to change from boundary layers dominant to bulk flow dominant. In addition to these experimental studies, some numerical studies such as that of Tsukahara *et al.* [8] have considered the effect of ribs on the global transport properties and flow characteristics for Reynolds number of 3.2×10^3 . The most important conclusion drawn from the research was that, the increment in the pressure drag due to roughness was dampened as a result of the strong adverse pressure gradient behind each rib. In [7, 8], the distance between two consecutive grooves (λ) was used as a key parameter and its influence on the mean flow and the friction coefficient was highlighted.

All the above cited studies were obtained with structural rough elements arranged in such a way as to obstruct the mean flow. This type of surface roughness is used either as heat transfer promoters or results from design necessity. They are known to be more efficient in generating friction drag than smooth surface. Rough elements aligned with mean flow is another category of surface roughness generally used to reduce the skin friction drag. This is achieved when the boundary layer thickness becomes smaller than the rough height and leading the flow resistance to be bulk dominant. The studies of Hall and Joseph [9], Moradi and Floryan [10], Greidanus *et al.* [11] and Zhu *et al.* [12] can be include in this category.

Understanding of the relevant mechanisms associated with an increase of friction drag in axially grooved cylinder flow involves a full understanding of the base flow *i.e.* the Taylor-Couette flow. Since the pioneering contribution of Couette [13], the Taylor-Couette flow has been greatly studied, both experimentally, numerically and theoretically because of its considerable scientific and engineering importance. The recent comprehensive review of Grossmann *et al.* [14] provides salient details on its fully developed turbulence regime from experimental, numerical, and theoretical points of view.

In this paper, we focus on statistical features of fully turbulent Taylor-Couette flow with axially grooved inner rotating cylinder. The grooves had a same rectangular shape and were regularly distributed on the tested cylin-

ders. In an attempt to investigate the effect of the groove density, we conducted series of experimental simulations using four different configurations. Three configurations of inner cylinder having 6, 12 and 24 grooves of a same rectangular shape and equally spaced in azimuthal direction were compared to a reference smooth cylinder. For each configuration, torque and pointwise velocity measurements were performed to assess global transport properties and flow characteristics. Section 2 describes the experimental setup, the geometry of each tested cylinder and the measurement techniques. The results are then analysed in section 3. The characteristics of the mean flow are summarized in section 3.1, with a focus on the noticeable effects of the groove density. The local flow characteristics are analysed in section 3.2, with a focus on the interaction of the groove and bulk flows. The torque results expressed in term of friction coefficient are discussed in section 3.3.

2. Experimental setup

2.1. Taylor-Couette facility

The experimental apparatus used has been specifically designed for the study of the Taylor-Couette flow. A detailed sketch and Photograph of this facility are given in Fig. 1. It comprised two coaxial cylinders that create a gap occupied by a working fluid. Each cylinder can rotate independently with the use of AC Servo motor (Panasonic, 1500 W). The outer cylinder made of 5 mm thick Plexiglas is driven via a driving belt while the inner cylinder is directly attached to a shaft through the torque sensor. The system is closed at the top end with a lid made in PVC and at bottom end with stainless steel lid and both ends rotating with the outer cylinder. The motors are controlled by a LabView software program that regulates the desired angular rotation rate of the corresponding cylinder. The radii of inner and outer cylinders are $r_i = 112.5$ mm and $r_o = 120$ mm, respectively, yielding to a gap of $d = r_o - r_i = 7.5$ mm and radii ratio of $\eta = r_i/r_o = 0.9375$. All the tested inner cylinders have a length $h = 200$ mm, which gives an axial aspect ratio of $h/d = 26.66$. The gaps between the top and bottom end-plates of the inner and outer cylinders are around 2.5 mm and 1.5 mm, respectively. All the results of this study concerns rotor/stator configurations, therefore the outer cylinder was kept at rest mechanically while varying the inner cylinder angular frequency ω_i . The relevant dimensionless parameters *i.e.* the parameter that characterizes the flow dynamic is the inner Reynolds number defined as:

$$Re_i = \frac{r_i \omega_i d}{\nu}. \quad (1)$$

2.2. Geometry of the inner cylinders

Our aim is to evaluate the action of axial grooves on the behaviour of Taylor-Couette flow, more precisely to identify possible mechanisms responsible for the flow resistance increasing. Thus three grooved inner cylinders

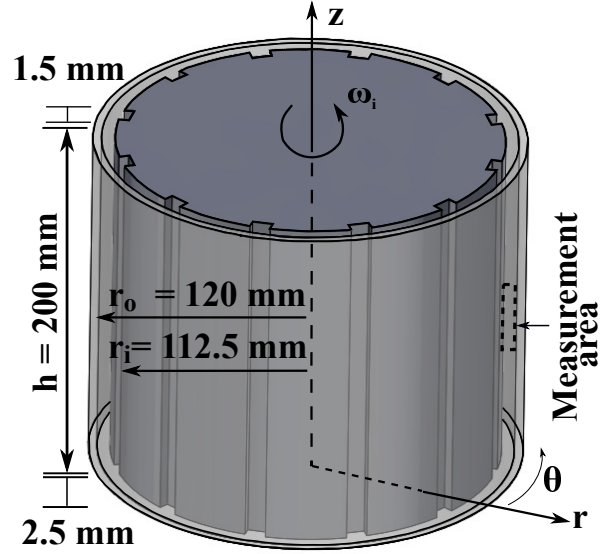
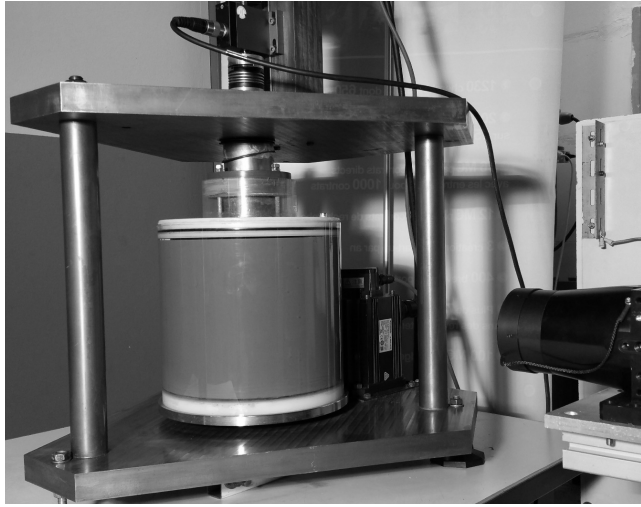


Figure 1: Photograph and sketch with dimensions of the experimental setup. Left: Taylor-Couette facility with torque meter at upper part of the picture and laser head at left side. Right: sketch showing the grooves of the inner cylinder and LDV Measurement area

were compared to a reference one having smooth surface. Note that for all the tested cases, the outer cylinder has a smooth surface.

Figure 2 presents the four inner-cylinder configurations. As can be seen, the grooved cylinders are equipped with 6, 12 or 24 identical axial rectangular cavities which were arranged periodically. They are named “ Gn ” where n is the number of the grooves. The detailed shape of the groove is shown at the bottom of Fig. 2. The ratio of the groove width $w = 12$ mm to its depth $k = 5.84$ mm is close to $w/k \simeq 2$. These parameters are motivated by the intended application, namely the investigation of aerodynamic losses in electric motor. The ratio of the groove separation distance $\lambda = 2\pi r_i/n$ to the groove depth k is generally used as the key parameter to distinguish the different wall roughness configurations [7, 8]. In the present work, λ/k for $G6$, $G12$ and $G24$ corresponds approximately to 20, 10 and 5, respectively.

2.3. Torque measurement

The torque (T) was measured on the inner cylinder using a co-rotating torque meter (KISTLER Ref.4503A, 10 N.m) with absolute precision of less than ± 0.02 N.m. As the torque meter is assembled in the shaft between the driving motor and the inner cylinder, the measuring torque includes the mechanical friction transmitted to the shaft through the bearings. This contribution is measured in case of air filled flow for all the rotating frequencies and subtracted from the total torque via linear interpolation. This contribution is less than 2% for all the runs. The present Taylor-Couette system is operated with water as working fluid at a initial temperature (T_f) in the range 20 – 24 °C, resulting in a volumetric mass density of $\rho = 998$ kg.m⁻³ and a kinematic viscosity of $\nu = 10^{-6}$ m².s⁻¹. The system is not equipped with the

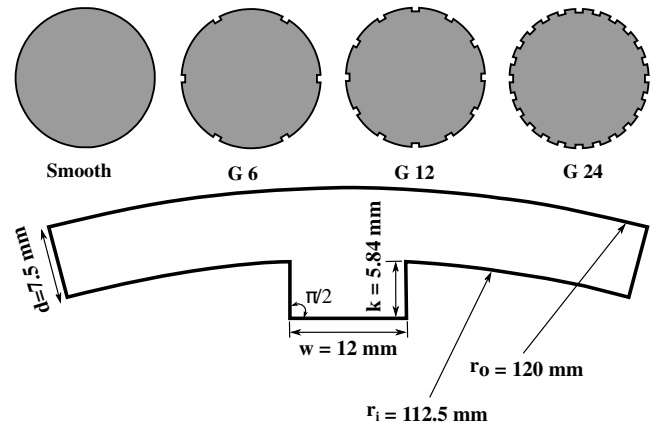


Figure 2: Schematic top view of the tested inner cylinders and the groove geometry. (Top), left to right reference smooth cylinder, cylinder with six ($G6$), twelve ($G12$) and twenty four ($G24$) grooves arranged at uniform spacing $\lambda = 2\pi r_i/n$; $n = 6, 12, 24$. (Bottom) Dimensions of elementary groove

temperature regulation unit, therefore, the mean temperature increases when the torque is sufficiently large yielding smaller viscosity than that of initial conditions. To compensate for the temperature dependence on fluid viscosity, K type thermocouple flash mounted under the top lid, in direct contact with the working fluid was used to measure the temperature rise due to frictional heating. The measured temperature allows to maintain a constant flow Reynolds number for all the experiments. For each run, the rotating frequency of inner cylinder was increased stepwise from 3.5 to 20 Hz at constant acceleration rate, $\partial Re_i / \partial \tau = 149102$ where τ is a non-dimensional time defined as $\tau = t\nu/d^2$. During each step, once the desired angular frequency was achieved, the torque, the angular frequency and the working fluid temperature were recorded simultaneously at sampling frequency of 5 kHz and sampling time of 40 s. The experiments were repeated three times for each inner cylinder over the same Reynolds number range to check the reproducibility. The repeatability were quite satisfactory, the variation being typically less than 2.5%. The measured torque is expressed in term of friction coefficient as follows:

$$C_f = \frac{T}{2\pi\rho r_i^2 h (r_i\omega_i)^2} \quad (2)$$

In the two horizontal gaps between the inner cylinder and the top or bottom lid, the fluid motion creates additional shear force. To estimate this contribution and subtract it from C_f , the empirical correlation developed by Hudson and Eibeck [15] in turbulent flow with single rotating disk and different shroud clearance ratios and gap aspect ratios was used. The contribution torque T_{disk} is expressed as follows:

$$T_{disk} = \frac{1}{2} C_{disk} \rho \omega_i^2 r_i^5, \quad (3)$$

with $C_{disk} = 2.83 (r_i^2 \omega_i / \nu)^{-0.48} (g/r_i)^{0.05}$. Here, g is the axial height of gap between the top or bottom endplates of the inner and outer cylinders. Extrapolating equation 3 to our parameters, end-effects contribution with respect to the measured torque was estimated to be in the ranges 9 – 17%, 7 – 12%, 6 – 11% and 4 – 8% for Smooth, G6, G12 and G24, respectively.

2.4. LDV measurement

The spatial distribution of the mean velocity in the meridional plane of the gap between the two cylinders (see Fig. 1) was measured by single-component Laser Doppler Anemometry (LDA), using a Dantec Dynamics FlowExplorer system, in a backscattering configuration. It consists of a 25 mW argon-ion laser with red wavelength (660 nm), 300 mm focal length of the fiber-optics probe given a measurement volume of $0.1 \times 0.1 \times 1 \text{ mm}^3$. The system has a high accuracy, as the calibration coefficient uncertainty is lower than 0.1%. The working fluid was seeded with iriodin 201 of 7 – 14 μm mean diameter used as the

tracer particles. For each inner cylinder, azimuthal and axial velocities were measured at 585 points distributed along 39 radial profiles at the mid-height of the rotational axis (see left part in Fig. 1) at constant axial intervals of 1 mm. At each measurement position, 100000 samples are acquired, with a limiting time acquisition of 40 s. The data rate lies in the range 800 – 10000 Hz, while the validation rate is upper than 60%. In dealing with velocity measurements in liquid Taylor-Couette flow by mean of LDA technique, the presence of flat or curved interface introduces a shift of the measurement volume and an underestimation of some components of the flow velocity (Huisman [16]). In this study a ray tracer have been used to calculate the measurement volume displacement and velocity correction factors. The velocity correction factor was applied only to the azimuthal velocity because, for the axial velocity, the laser beams were normal to the flat plate therefore the difference in refractive index is balanced by the changing wavelength.

3. Results and discussion

3.1. Mean flow characteristics

Prior to examining the friction coefficient, we investigate the effect of groove on the overall behaviour of the bulk flow. To characterize the turbulent states in the grooved and smooth cases, we performed scans of the azimuthal and axial velocities in the meridional plane (r, z) at mid-height of the apparatus for two Reynolds number $Re_i = 47000$ and 80000 . At these Reynolds numbers, the flow is considered as fully turbulent. Modified dimensionless radial coordinate $r^+ = (r - r_i)/d$ was used so that the inner cylinder is at $r^+ = 0$ while the outer cylinder is at $r^+ = 1$. The wall inner cylinder velocity $r_i\omega_i$ was used as velocity scale. The data of smooth cylinder served as baseline data against those of grooved cylinders.

Figure 3 compares four time-averaged azimuthal and axial velocity contour plots for $Re_i = 47000$, showing the flow characteristics with respect to the inner cylinder surface structures. In the case of smooth surface, the presence of large-scale structures was clearly highlighted by radial inflow and outflow boundaries visible on azimuthal velocity field (see top part in Fig. 3 (a)) and, the alternation of positive and negative velocity visible on axial velocity field (see bottom part in Fig. 3 (a)). From these boundaries, high-speed fluid near the inner cylinder and low-speed fluid near the outer cylinder are ejected in the bulk regions between the vortices and contribute to redistribute the angular momentum. The elliptical shape of these vortices depends on the strength of inward and outward fluid. According to Tokgoz *et al.* [16] the birth and death of new vortices always takes place at these boundaries. For the present geometry constraints, Reynolds number and acceleration rate ($\partial Re_i / \partial \tau$), the local axial wavelength of the vortices obtained at mid-height of the apparatus was around $4.4d$, comparable to the value reported by Ravelet *et al.* [17] for

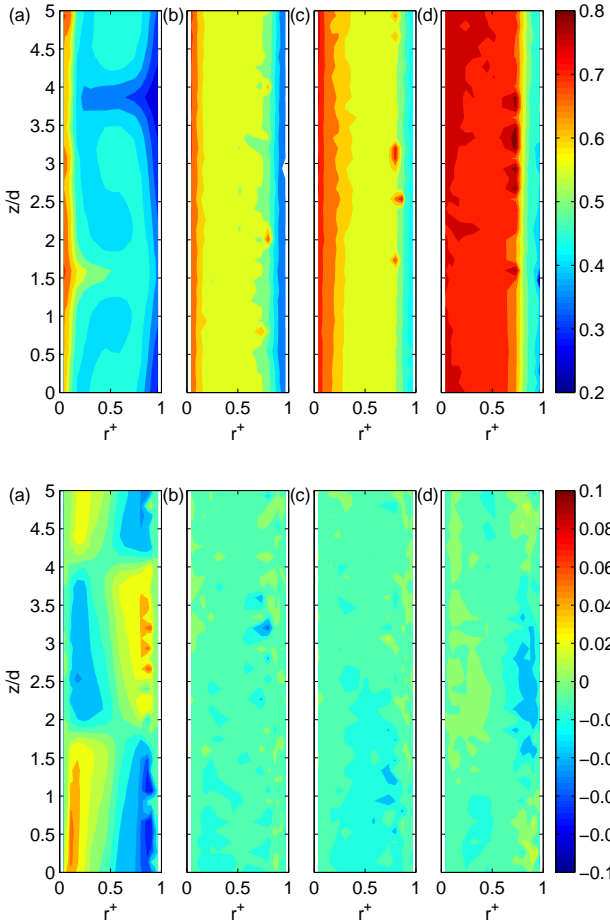


Figure 3: (Colour online) Contour plots of the time-averaged normalized azimuthal (top) and axial (bottom) velocity fields V_{θ} measured by LDA at Reynolds number $Re_i = 47000$. (a) Smooth case, (b) $G6$ case, (c) $G12$ case, and (d) $G24$ case

$Re_i = 14000$ in an experiment with slightly different gap ratio.

The three grooved cylinder results revealed certain constants in the behavior of the velocity fields and notable structural differences compared to smooth surface case. Contrary to the smooth cylinder, no axial periodicity was observed indicating the absence of large coherent structures. As expected, the grooves produces radial velocity modulations and the resulting interaction with the bulk flow breaks the primary instability responsible of Couette-Taylor roll formation. The random distribution of the axial velocity confirmed the breakdown of coherence and the small scale structures of the flows. Also from the axial velocity field, one can state that there was negligible convective transport or diffusion of azimuthal momentum in the bulk flow. From comparison between the grooved surface cases, one can notice that, the region of high azimuthal velocity near the inner cylinder gradually extended into the bulk flow with increasing the groove number (see top part in Fig. 3 (b-d)) and, the azimuthal velocity became more uniformly distributed along the axial direction. The

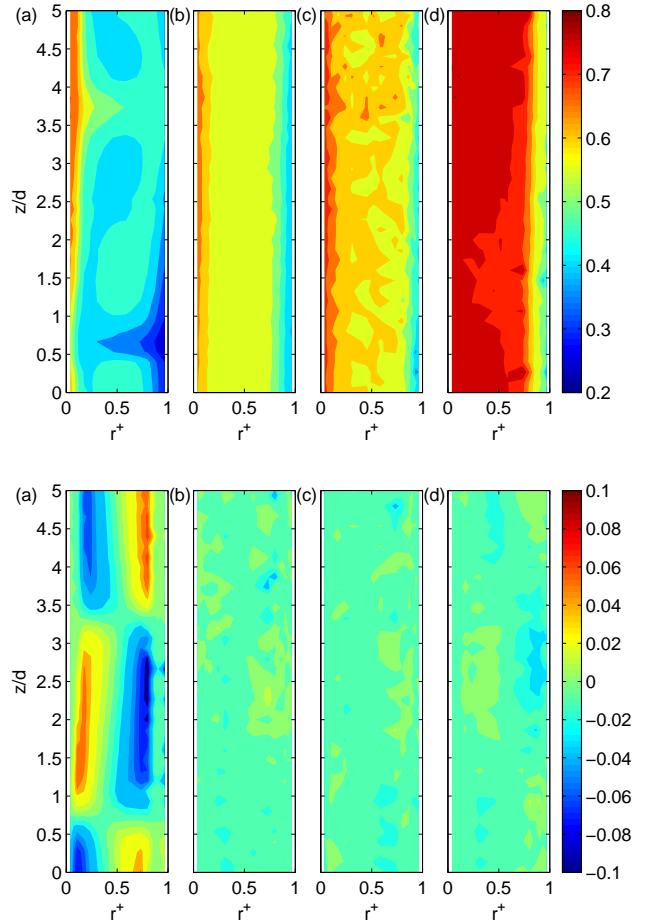


Figure 4: (Colour online) Contour plots of the time-averaged normalized azimuthal (top) and axial (bottom) velocity fields V_{θ} measured by LDA at Reynolds number $Re_i = 80000$. (a) Smooth case, (b) $G6$ case, (c) $G12$ case, and (d) $G24$ case

change in magnitude of azimuthal velocity in the bulk is not fully understood. However, in our opinion, it may result from ejection of high-speed fluid at the top edges of each groove. In fact, the flow separation occurring at the top edges of the grooves may generate a radial high-speed fluid ejection towards the outer cylinder. As the groove number increased, the contribution of the ejected fluid will increase, explaining the changes observed in magnitude of the azimuthal velocity contours.

In order to check the flow structure dependence on the Reynolds number, Fig. 4 compares four time-averaged azimuthal and axial velocity contour plots at $Re_i = 80000$. At this Reynolds number, the average flow with grooved wall shares common features with those at $Re_i = 47000$, such as the loss of axial periodicity and the increase in magnitude of azimuthal velocity in the bulk as the groove number increased. The only noticeable difference was a large local axial wavelength of around $6d$ obtained with the smooth surface case. Based on these results, we can rigorously claim that, this specific axial groove geometry enhances the momentum transport in the radial direc-

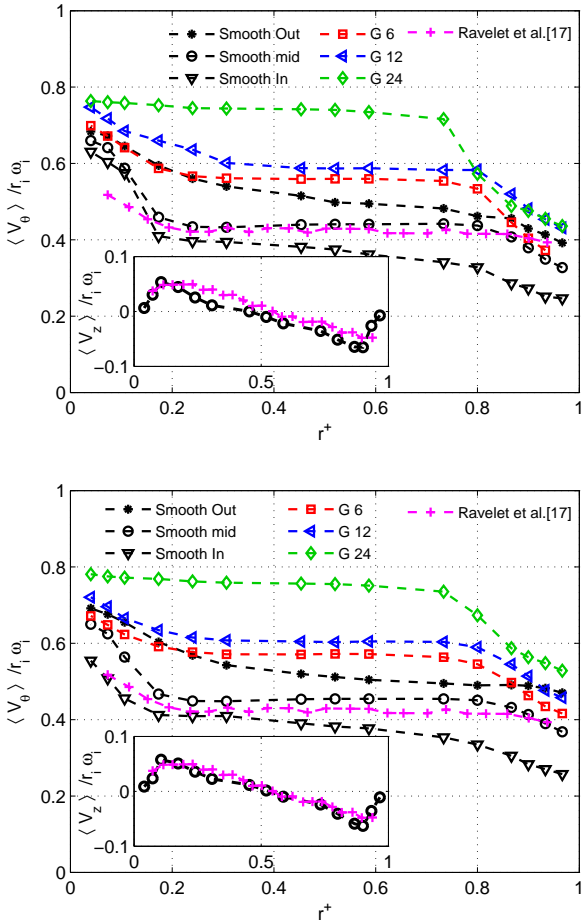


Figure 5: Normalized averaged azimuthal (V_θ) and axial (V_z) velocity profile along radial coordinate for Reynolds number $Re_i = 47000$ (top) and $Re_i = 80000$ (bottom). The three grooved cylinder profiles have been averaged over both time and axial position. The smooth surface profiles were extracted at the center of a vortex (labelled Smooth mid), inflow (labelled Smooth In) and outflow (labelled Smooth Out) boundaries between two consecutive vortices. The sub-figure displays the axial velocity profile extracted at the center of a vortex. Comparison to the data of Ravelet *et al.* [17]

tion *i.e.* from the inner cylinder to the bulk flow at high Reynolds number.

In Fig. 5 we compare profiles of the mean azimuthal velocity across the gap between the cylinders for the two Reynolds numbers. The three grooved cylinder profiles have been averaged along the axial position. The smooth surface profiles were extracted at three relevant locations, *i.e.* the center of a vortex, and two consecutive vortex boundaries where the fluid is ejected towards the bulk flow. The data of Ravelet *et al.* [17] was added for comparison. Globally, the overall trend of the present profiles was comparable with Ravelet *et al.* [17] results. The slight gap observed on the azimuthal velocity profile was probably due to Reynolds number or radii ratio dependence. A strong signature of the number of the grooves could be seen on these profiles as mentioned previously. As the groove number increased, the profiles became more flat near the rotat-

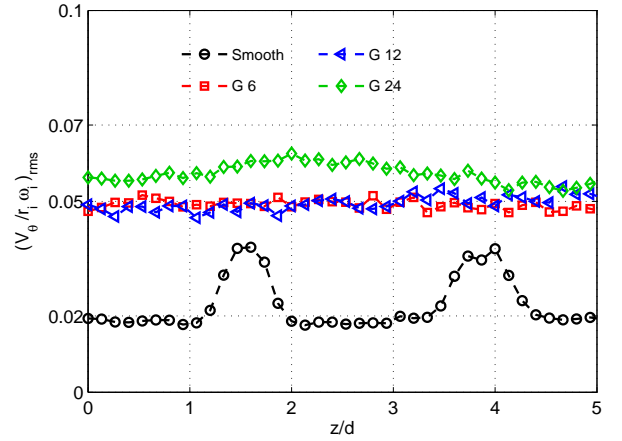


Figure 6: Normalized root mean square azimuthal velocity profile along axial coordinate for Reynolds number $Re_i = 47000$. The profiles have been averaged radially in bulk flow

ing cylinder, yielding to a steeper velocity gradient. This corresponds to the so-called downward shifts in the log-law region, as it is well established that any rough surface leads to a downward shift in the logarithmic region of the velocity profile ([18, 19]). The increase in the azimuthal velocity, averaged axially at mid-gap was constant for the two Reynolds numbers and was approximately 27%, 33% and 68% of the smooth case value for G6, G12 and G24, respectively. The bulk azimuthal velocity increase in the presence of wall roughness were also reported from experimental data by Greidanus *et al.* [11] and numerical data by Hayase *et al.* [1] and Zhu *et al.* [12]. The latter authors attributed it to the conservation of the angular velocity current along the radius.

To gain some insight on the velocity fluctuations, the root mean square azimuthal velocity profiles extracted at mid-gap in the bulk flow are plotted against the axial coordinate in Fig. 6 for Reynolds number $Re_i = 47000$. We do not include the profiles for $Re_i = 80000$ because they were identical to those at $Re_i = 47000$. As expected the grooves not only impacted the mean flow, but also the fluctuations. The three grooved cylinders exhibited nearly constant value along the axial direction, with a slightly higher intensity for G24. For the smooth cylinder, the profiles exhibited a prominent double-peak feature characteristic of the inflow and outflow boundaries of Taylor vortices. Its mean intensity was lower than those of the grooved cylinders. Globally, such behaviours were consistent with those of mean flow and could be attributed to competing factors of groove-induced modulations that adding periodically intermittency or heterogeneity in bulk flow.

3.2. Local flow characteristics

In order to perform spectral analysis of the flow unsteadiness, time-resolved signals of the azimuthal velocity have been recorded at a mean acquisition frequency of

around 10 kHz and maximum point time series of 1000000. These parameters correspond to approximately 1132 and 662 points per revolution of the inner cylinder for $Re_i = 47000$ and $Re_i = 80000$, respectively. Before computing Fourier transform, all LDV signals were reconstructed on an equally spaced time grid based on local mean sampling frequency via zeroth-order interpolation. All the power spectra were estimated using the periodogram technique with a Hanning window and an overlapping of 50%. Each spectrum was expressed in decibels (dB) using the following formula:

$$S(f) = 20 \log_{10}(p(f)/p_0), \quad (4)$$

where $P(f)$ is the power spectrum density function and P_0 is taken equal to unity. The frequency was normalized by the groove passing frequency $f_{gpf} = n\omega_i/2\pi$.

Figures 7 and 8 compare the power spectra of the azimuthal velocity fluctuation at three measured points distributed across the flow, one in the bulk flow and two others near the inner and outer cylinder boundary layers. These figures help observing the flow dynamics in more details. Near the inner cylinder at $r^+ = 0.1$, for both Reynolds numbers, the spectra exhibited seven strong discrete peaks, illustrating the complexity of the near-wall flow. The first peak, at $f = f_{gpf}$, was associated with the groove passing frequency, whereas the others correspond to its harmonics. At this location, the distribution of turbulent energy between the different harmonics depends on the groove number. It should be recalled that the appearance of harmonics typifies non linearities generally associated with the creation of turbulence. The energy content for G6 was quasi-constant for all the harmonics (see Figs. 7 (a) and 8 (a)), while it gradually attenuates for G12 and G24. We related it to the distance between the grooves, not sufficient for the flow to be recovered, so leading to complex unstable flow. In the bulk flow at $r^+ = 0.55$, the influence of the groove became slightly weaker. Apart from the groove passing frequency, the spectra displayed approximately three, one and zero low energy peaks (see Figs. 7 (b) and 8 (b)) for G6, G12 and G24, respectively. This is consistent with observations at $r^+ = 0.1$ about the dependence of the groove signature on its number. With a deeper penetration *i.e.* at $r^+ = 0.8$, the energy content of the peak was gradually diminished and the peaks were completely suppressed for G12 and G24 (see Figs. 7 (c) and 8 (c)). For the two cases, the disappearance of the sharp peaks does not imply necessary that the flow is totally featureless in this region. The large value of λ (distance between two consecutive grooves), ensures a low interaction between consecutive groove modulated waves, probably responsible for the persistence of the peak in G6 flow.

Flow characteristic analysis based on spectra indicated different local dynamics in relation to groove number and spatial location. In the following, we propose to go further in performing spatial analysis using phase-average technique. The LDV signals reconstructed via zeroth-order

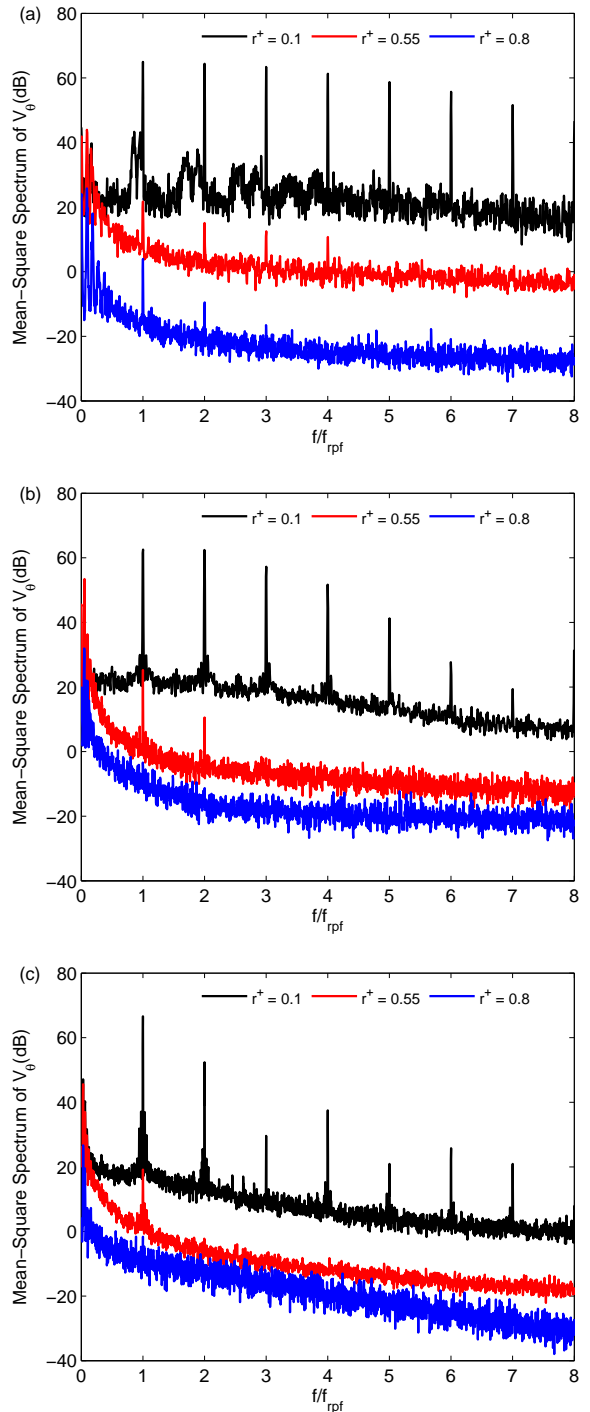


Figure 7: Square amplitude spectra of tangential velocity $V_\theta(t)$ at three different locations for Reynolds number $Re_i = 47000$. The first and the third spectrum is shifted 13.98 dB upward and -26 dB downward with respect to the middle one, respectively. (a) G6 case, (b) G12 case, and (c) G24 case

interpolation at mean sampling frequency f_{acq} were decomposed into N (integer number) revolutions of period $\tau = 2\pi/\omega_i$. Each period contains $K = 2\pi f_{acq}/\omega_i$ samples, where K is an integer. From the velocity phase-averaged at $\phi = j\omega_i/f_{acq}$ ($j = 1, \dots, K$), we define the mean (Eq. 5)

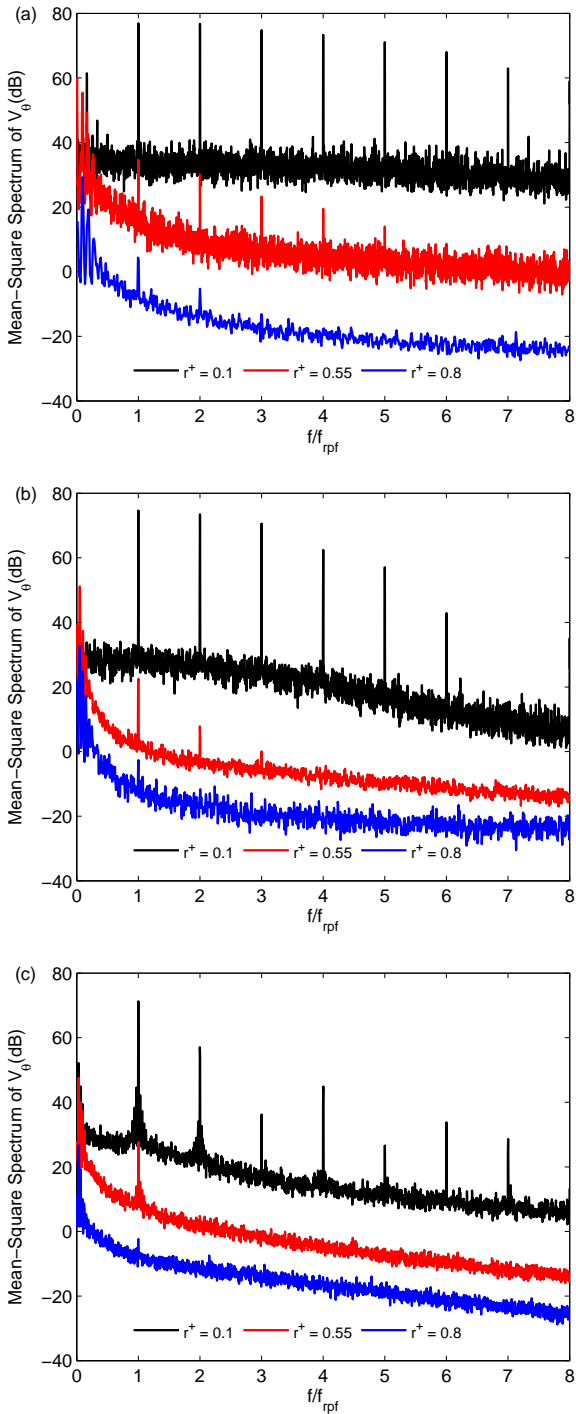


Figure 8: Square amplitude spectra of tangential velocity $V_\theta(t)$ at three different locations for Reynolds number $Re_i = 80000$. The first and the third spectrum is shifted 13.98 dB upward and -26 dB downward with respect to the middle one, respectively. (a) $G6$ case, (b) $G12$ case, and (c) $G24$ case

and standard deviation (Eq. 6) of azimuthal velocity:

$$\langle V_\theta(\phi) \rangle = \frac{1}{N} \sum_{i=0}^{N-1} V_\theta(\phi + i\tau), \quad \phi \in [0, 360]^\circ, \quad (5)$$

$$RMS\langle V_\theta(\phi) \rangle = \frac{1}{N} \sum_{i=0}^{N-1} V_\theta(\phi + i\tau), \quad (6)$$

In Fig. 9, we compare profiles of the phase-averaged azimuthal velocity normalized by the rotation velocity of the

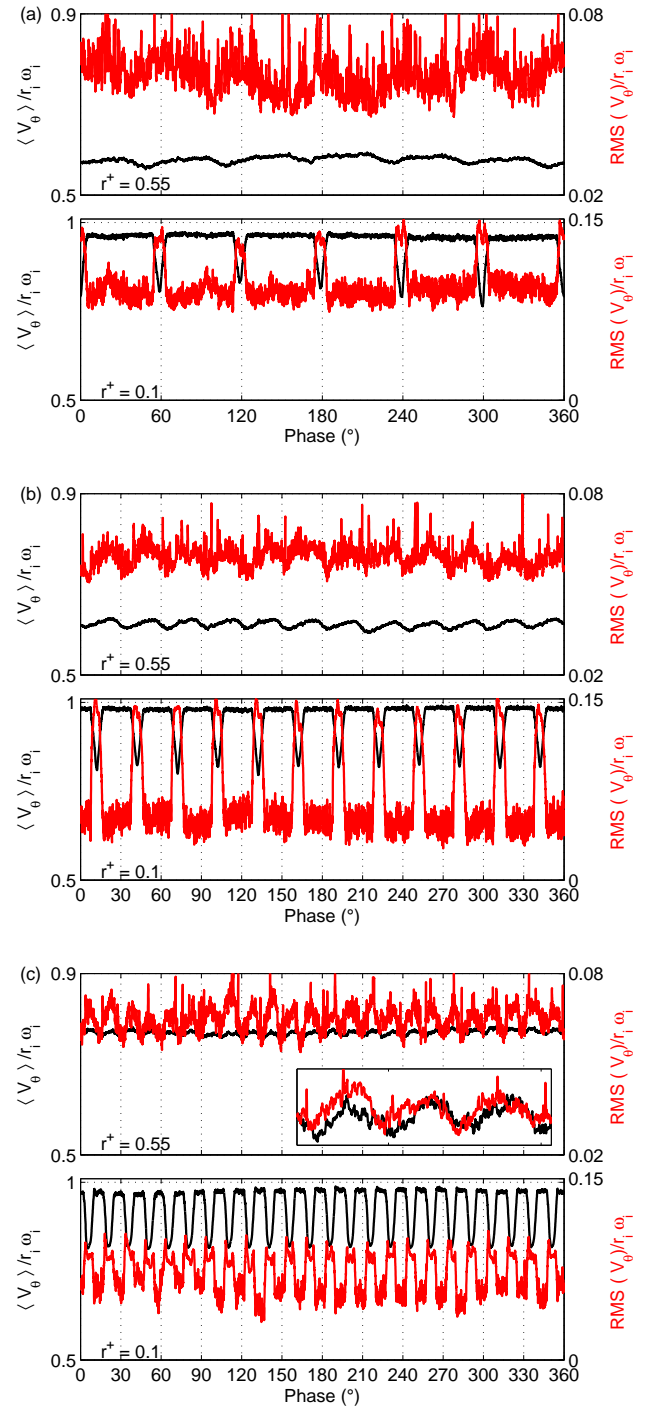


Figure 9: Normalized phase-averaged azimuthal velocity for $Re_i = 47000$: mean $\langle V_\theta(\phi) \rangle / r_i \omega_i$ (black) and root mean squared $RMS\langle V_\theta(\phi) \rangle / r_i \omega_i$ (red). (a) $G6$ case, (b) $G12$ case, and (c) $G24$ case. The phase-averaged technique was applied only for the two locations where the spectrum density displays at least one discernible peak

inner cylinder wall. Only the case $Re_i = 47000$ was shown since the distribution was identical for the two Reynolds numbers. The signature of the groove can be observed in both near-wall and bulk flow locations. Near the rotating wall at $r^+ = 0.1$, the profiles of mean azimuthal velocity were highly periodic and regular with only a single dominant frequency corresponding to groove passage. The periodicity were 60° , 30° and 15° for $G6$, $G12$, and $G24$, respectively. The profiles also showed that, the mean flow near the inner cylinder was dominated by the velocity deficit created by the groove passages. This can be explained by the presence of the steady recirculation flow in the groove. In fact, literature data based on the channels flow with rectangular cavities [18, 19] or Taylor-Couette flow with grooved inner or outer cylinder [1] revealed a recirculating flow within the cavities. The presence of this recirculating flow will induced by viscous force a shear zone at each groove passage, which will result in the azimuthal velocity deficit. Another interesting observation revealed by phase-averaged technique was the higher fluctuation level within the velocity deficit region. This observation is a consequence of a higher shear stress and velocity gradient induced by the cavity shear layer which generate an intense turbulent production. The phase-averaged profiles in the bulk flow at $r^+ = 0.55$ showed weakness of groove signatures as compared to $r^+ = 0.1$. The fluctuation level was more attenuated and its maximum location was shifted to center of the crest, contrary to what happen at $r^+ = 0.1$.

3.3. Torque

The torque of the four inner cylinders expressed in terms of friction coefficient C_f (see equation 2) is shown in Fig. 10 as a function of Reynolds number Re_i . In this figure we show also local scaling exponent α distribution estimated by mean of logarithmic derivative. Before we discuss the variation of the friction coefficient with the groove number, we compare our smooth cylinder data to experimental results of Ravelet *et al.* [17], Motozawa *et al.* [7] and Lewis and Swinney [20] and, to an empirical correlation of Dubrulle and Hersant [21]. The large gap between the present smooth data and those of literature is not surprising since rigorous direct comparison could not be achieved owing to the different gap ratios of the experiments and the end effects. It should be noted however that the torque was measured in same way in [17, 7] and in current study, the torque was corrected from end effects by dividing by 2 in [17] and by using the correlation of Hudson and Eibeck [15] in the present study. No end effects correction was used in [7, 20] since in [20], the authors measured the torque acting only on the central part of the inner cylinder. To obtain good agreement with the correlation of Dubrulle and Hersant [21] rewritten as

$$C_f = \frac{K_7}{2\pi} \frac{(1-\eta)^{1/2}}{\ln[\eta^2(1-\eta)Re_i^2/K_8]^{3/2}}, \quad (7)$$

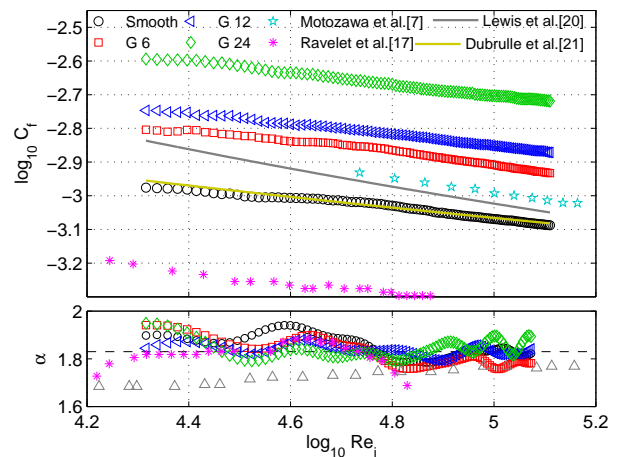


Figure 10: Friction coefficient C_f and local exponent α against Reynolds number Re_i . α is defined by power law $C_f \propto Re_i^{2-\alpha}$ and estimated as $\alpha = 2 + d \log(C_f) / d \log(Re_i)$. Comparison to the experimental data of Ravelet *et al.* [17] ($\eta = 0.917$), Motozawa *et al.* [7] ($\eta = 0.939$) and Lewis and Swinney [20] (equation 3, $\eta = 0.724$), and the empirical correlation of Dubrulle and Hersant [21](equation 10) fitted to our data with $K_7 = 1.95$ and $K_8 = 10^0$

we use $K_7 = 1.95$ and $K_8 = 10^0$ which should be compared to the given values of $K_7 = 0.5$ and $K_8 = 10^4$. It should be recalled that Dubrulle and Hersant [21] constructed their correlation using results of Lewis and Swinney [20] obtained with $\eta = 0.724$.

We now analyse the influence of the groove number on the friction coefficient in relation with Reynolds number. As indicated in Fig. 10, the friction coefficient increased with increasing groove number. Their profiles were quite similar in shape without discernible transitional regime, which means the flow being at fully developed turbulence state over the range of Reynolds numbers examined. The local scaling exponent (see bottom Fig. 10) also confirmed this regime. The exponent for all the three grooved cylinders collapsed with smooth cylinder exponent, with mean value of 1.83 ± 0.1 . This value agreed well with the results of Lathrop *et al.* [22], Lewis and Swinney [20] and Ravelet *et al.* [17]. In the previous experimental studies of $C_f \propto Re_i^{2-\alpha}$ (Cadot *et al.* [5], van den Berg *et al.* [23]), it was found that the value of the exponent α was equal to 1.88 with an inner cylinder roughened by parallel regular square cross section ribs and outer smooth cylinder, and $\alpha = 2$ when both walls were rough. However our inner grooved cylinder exponents were fairly close to $\alpha = 1.88$, the fact that α was approximately equal to smooth cylinder value points out that the effects of grooves on the exponent might be too weak to be observed due to the large value of η or, the contribution of grooves might be associated to a simple shift in pressure drag. Therefore one may conclude that the present friction coefficient scaling is not bulk flow dominant contrary to the common behaviour of classical rough wall.

To further illustrate the effect of groove number on

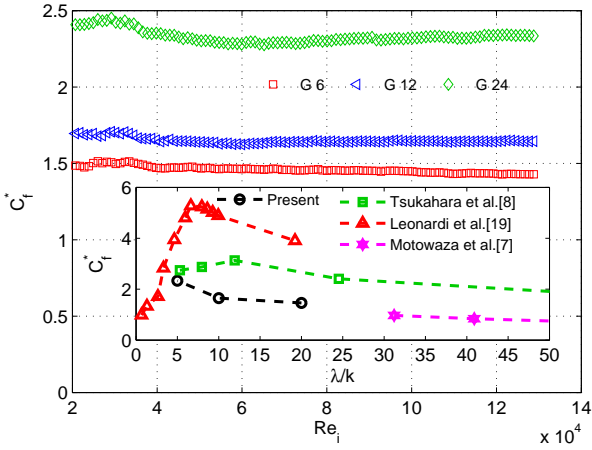


Figure 11: friction coefficient ratios between the grooved and smooth cylinders $C_f^* = C_f/C_{f,smooth}$ as a function of Re_i . Insert: C_f^* averaged over Re_i as a function of rough element interval normalized by its height λ/k . Comparison to, DNS study of turbulent channels flow with transverse square ribs of leonardi *et al.* [19], experimental and DNS results of Taylor-Couette flow with triangular and square longitudinal ribs of Motozawa *et al.* [7] and Tsukahara *et al.* [8], respectively

the torque, Fig. 11 presents the ratio of friction coefficients between the grooved and smooth cylinders $C_f^* = C_f/C_{f,smooth}$ as a function of Re_i . The friction ratio was approximately constant across the whole Reynolds number range studied. Averaged over the whole Re_i range, the mean ratio C_f^* was approximately 1.46, 1.65 and 2.33 times higher for $G6$, $G12$, and $G24$, respectively. In Fig. 11, the subfigure compares the mean ratios C_f^* to those of literature [19, 7, 8] as function of rough element interval normalized by its height λ/k . Significant differences can be observed. The grooved cylinder values were found to be lower on average than the ribbed channel and cylinder results for all λ/k and, the peak was also shifted towards lower λ/k . In view of present results, we can assume that the higher friction coefficient ratio in [19, 7, 8] can be attributed to enhanced pressure drag by rib. Indeed, for these studies, the main flow direction is obstructed by the ribs. As a result, a strong pressure gradient is generated leading to intense transfer of momentum from fluid to the wall.

To go further in the analysis, effort is made to estimate the relative contribution of single groove by mean of two assumptions: (i) the groove (cavity) contribution to the skin friction is considered negligible compared to that of the crest; (ii) the skin friction on the crest is equal to that of smooth cylinder over the Reynolds number range. Under the two assumptions, the contribution of single groove is defined as follows:

$$C_{f,1G} = \frac{C_f - \frac{S_{Gn}}{S_{smooth}} C_{f,smooth}}{n}, \quad (8)$$

where S_{smooth} is lateral surface area of smooth cylinder and S_{Gn} is a crest surface area of G_n cylinder. $C_{f,1G}$ can

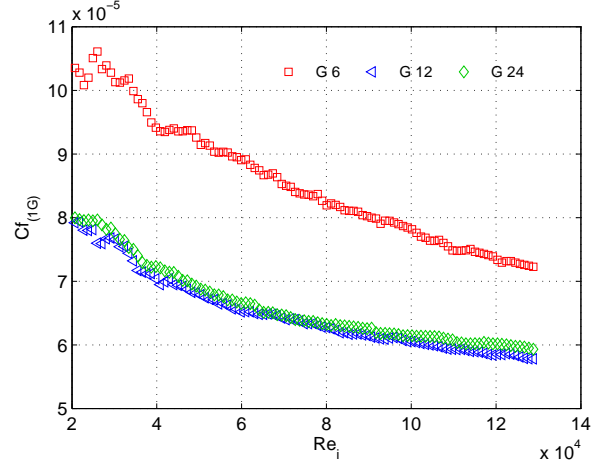


Figure 12: Relative contribution of single groove $C_{f,1G}$ as a function of Re_i

be interpreted as a single groove pressure drag contribution to the total friction coefficient. Figure 12 shows the relative contribution of single groove as a function of Re_i . The profiles were similar in shape for the three tested cylinders, even though they illustrated a substantial dependence on Reynolds number. The contribution should be equal for the three cases if our assumptions are strictly valid or if there are no interaction between the groove-induced modulation. The first assumption is supported by the literature results of Hayase *et al.* [1] and leonardi *et al.* [19] obtained with pitch ratio less than 4 which is the case of the current study ($w/k \approx 2$). The second assumption is slightly weaker since the velocity results (see Fig. 3, 4 and 5) clearly showed a steeper velocity gradient and an increase of azimuthal bulk velocity with increasing groove number. They will result in skin friction reduction on the crest *i.e.* the reduction of the boundary layer contributions. The gap between $G12$ and $G24$, and $G6$ distributions was too large to be associated only with reduction of skin friction on the crest. Based on these observations and arguments, we conclude that $G12$ and $G24$ flows have similar structural behaviour, strictly different from that of $G6$, which we associated to groove density. The azimuthal velocity spectra (see Fig. 7, 8) also confirmed the difference in the flow feature since the groove signature was found to persist until the near wall of the outer cylinder for $G6$, which was not the case for $G12$ and $G24$. This agrees well with the finding of Tsukahara *et al.* [8] who observed that, for $\lambda/k \geq 13$, the rough elements were isolated. Globally, similar behaviour was reported by Motozawa *et al.* [7] for ribbed inner cylinder, which the authors attributed to the recovery of the velocity distribution which could not be achieved for smaller value of λ/k .

We therefore conclude that, for this type of flow configuration where surface morphology significantly acts on the global transport properties represented by measured torque, at least spatial distribution of velocity field at

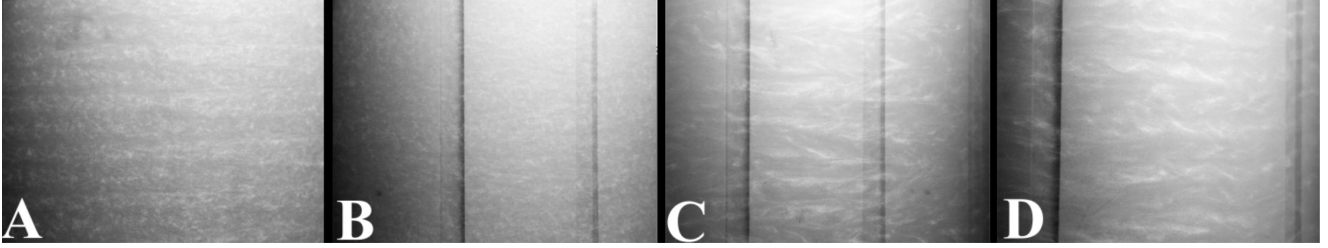


Figure 13: Photographs of the flow at different Reynolds number and surface roughness. A: smooth cylinder at $Re_i = 4.06 \times 10^3$, B: $G12$ cylinder at $Re_i = 4.06 \times 10^3$, C: $G12$ cylinder at $Re_i = 1.15 \times 10^3$, D: $G6$ cylinder at $Re_i = 1.15 \times 10^3$. The flow structure is visualized using microscopic iridol particles

vicinity of wall should be derived from more complete experiments, to account for the separate effects of elementary rough element on skin friction and pressure drag, which is not the case of the current study.

4. Conclusion and future work

Derived from industrial situations, the experimental conditions led to the study of Taylor Couette flow with axially grooved rotating inner cylinder and fixed outer cylinder. With a large radius ratio and high Reynolds number up to $Re_i = 13 \times 10^4$, this experiment simulated a compact electric motor behaviour at high velocity speed where intense heat transfer took place. Torque and pointwise velocity measurements were carried out for different tested inner cylinders to assess flow characteristics and global transport properties.

The most prominent differences in the flow features between the grooved tested cylinder cases and the smooth cylinder case were, a loss of axial-dependency of the time-averaged velocity field, a steeper velocity gradient near the grooved rotating cylinders and an increase of the bulk flow azimuthal velocity with decreasing a circumferentially periodic length λ/k . This parameter was found to discriminate the flow feature since it allowed to characterize the periodic spatial variations in the flow within the roughness boundary and the bulk flow.

Direct consequence of these variations in the flow features was a large difference in global transport properties measured by mean of global torque and expressed in term of friction coefficient. It was shown that the use of grooved inner cylinder increased the friction coefficient and the groove contribution rate was a function of λ/k . Within the Reynolds number range of this study ($2 \times 10^4 \leq Re_i \leq 13 \times 10^4$), the friction coefficient ratio between the rough and the smooth cylinders was approximately constant and the mean ratio was approximately 1.46, 1.65 and 2.33 times higher for $G6$, $G12$, and $G24$, respectively. Despite these strong effects on the measured torque, the computed local exponent seemed insensitive, contrary to the common behaviour of classical rough wall.

The current study must be only the start of a long experimental program to further explore the effects of axial rectangular groove on turbulent Taylor-Couette flow.

The most immediate and urgent objective will be to perform high spatial resolution velocity measurement in the rotating grooved inner cylinder sublayers in order to estimate local contribution of skin friction and pressure drag. It should be noted that all of the experiments were conducted for a single value of pitch to height ratio ($w/k \approx 2$). Hence, future experiment should be performed for different values of w/k to confirm our observations.

The next step will be to examine the flow dynamics and the transport properties in low Reynolds number range. In fact, it is interesting to observe in Fig. 13 that different turbulent states coexist. At $Re_i = 4.06 \times 10^3$, the smooth cylinder flow was dominated by Taylor-vortices while the $G12$ flow did not contain obvious structures like Taylor-vortices. By decreasing the Reynolds number from $Re_i = 4.06 \times 10^3$ to $Re_i = 1.15 \times 10^3$, a bifurcation process occurred for $G12$ flow (see Fig. 13 C) revealed by the presence of large coherence structures with azimuthal wavelengths locked to λ . This is confirmed by the Photograph in Fig. 13 D obtained with $G6$. This kind of study has been performed by Ravelet *et al.* [24] in inertially driven von Kármán closed flow in which the authors observed the so-called 'turbulent bifurcation' and multistability. The objective will be to check whether these flow features and bifurcation are reflected in the overall transport properties.

References

- [1] T. Hayase, J. A. C. Humphrey, R. Greif, Numerical calculation of convective heat transfer between rotating coaxial cylinders with periodically embedded cavities, *Journal of Heat Transfer* 114 (1992) 589–597. doi:10.1115/1.2911322.
- [2] Y. N. Lee, W. Minkowycz, Heat transfer characteristics of the annulus of two coaxial cylinders with one cylinder rotating, *International Journal of Heat and Mass Transfer* 32 (1989) 711–722. doi:http://dx.doi.org/10.1016/0017-9310(89)90218-4.
- [3] S. Gardiner, R. Sabersky, Heat transfer in an annular gap, *International Journal of Heat and Mass Transfer* 21 (1978) 1459–1466. doi:http://dx.doi.org/10.1016/0017-9310(78)90002-9.
- [4] M. Fnot, Y. Bertin, E. Dorignac, G. Lalizel, A review of heat transfer between concentric rotating cylinders with or without axial flow, *International Journal of Thermal Sciences* 50 (2011) 1138–1155. doi:http://dx.doi.org/10.1016/j.ijthermalsci.2011.02.013.
- [5] O. Cadot, Y. Couder, A. Daerr, S. Douady, A. Tsinober, Energy injection in closed turbulent flows: Stirring through boundary

- layers versus inertial stirring, *Physical Review E* 56 (1997) 427–433. doi:10.1103/PhysRevE.56.427.
- [6] T. H. van den Berg, C. R. Doering, D. Lohse, D. P. Lathrop, Smooth and rough boundaries in turbulent taylor-couette flow, *Physical Review E* 68 (2003) 036307. doi:10.1103/PhysRevE.68.036307.
- [7] M. Motozawa, T. Ito, K. Iwamoto, H. Kawashima, H. Ando, T. Senda, Y. Tsuji, Y. Kawaguchi, Experimental investigations on frictional resistance and velocity distribution of rough wall with regularly distributed triangular ribs, *International Journal of Heat and Fluid Flow* 41 (2013) 112–121. doi:http://dx.doi.org/10.1016/j.ijheatfluidflow.2013.03.004.
- [8] T. Tsukahara, M. Ishikawa, Y. Kawaguchi, Dns study of the turbulent taylor-vortex flow on a ribbed inner cylinder, *Advances in Mechanical Engineering* (2013) 628490doi:10.1155/2013/628490.
- [9] T. Hall, D. Joseph, Rotating cylinder drag balance with application to riblets, *Experiments in Fluids* 29 (2000) 215–227. doi:10.1007/s003489900075.
- [10] H. V. Moradi, J. M. Floryan, Flows in annuli with longitudinal grooves, *Journal of Fluid Mechanics* 716 (2013) 280–315. doi:10.1017/jfm.2012.547.
- [11] A. J. Greidanus, R. Delfos, S. Tokgoz, J. Westerweel, Turbulent taylor-couette flow over riblets: drag reduction and the effect of bulk fluid rotation, *Experiments in Fluids* 56 (2015) 107. doi:10.1007/s00348-015-1978-7.
- [12] X. Zhu, R. Ostilla-Mnico, R. Verzicco, D. Lohse, Direct numerical simulation of taylorcouette flow with grooved walls: torque scaling and flow structure, *Journal of Fluid Mechanics* 794 (2016) 746–774. doi:10.1017/jfm.2016.179.
- [13] M. Couette, Etude sur le frottement des liquids, *Annales de chimie et de physique* 21 (1890) 433–510.
- [14] S. Grossmann, D. Lohse, C. Sun, High reynolds number taylorcouette flow, *Annual Review of Fluid Mechanics* 48 (2016) 53–80.
- [15] A. J. Hudson, P. A. Eibeck, Torque measurements of corotating disks in an axisymmetric enclosure, *Journal of Fluids Engineering* 113 (1991) 648–653. doi:10.1115/1.2926529.
- [16] S. G. Huisman, D. P. van Gils, C. Sun, Applying laser doppler anemometry inside a taylor-couette geometry using a ray-tracer to correct for curvature effects, *European Journal of Mechanics - B/Fluids* 36 (2012) 115–119. doi:http://dx.doi.org/10.1016/j.euromechflu.2012.03.013.
- [17] F. Ravelet, R. Delfos, J. Westerweel, Influence of global rotation and reynolds number on the large-scale features of a turbulent taylorcouette flow, *Physics of Fluids* 22 (2010) 055103. doi:10.1063/1.3392773.
- [18] A. E. Perry, W. H. Schofield, P. N. Joubert, Rough wall turbulent boundary layers, *Journal of Fluid Mechanics* 37 (2) (1969) 383–413. doi:10.1017/S0022112069000619.
- [19] S. Leonardi, P. Orlandi, R. J. Smalley, L. Djenidi, R. A. Antonia, Direct numerical simulations of turbulent channel flow with transverse square bars on one wall, *Journal of Fluid Mechanics* 491 (2003) 229–238. doi:10.1017/S0022112003005500.
- [20] G. S. Lewis, H. L. Swinney, Velocity structure functions, scaling, and transitions in high-reynolds-number couette-taylor flow, *Physical Review E* 59 (1999) 5457–5467. doi:10.1103/PhysRevE.59.5457.
- [21] B. Dubrulle, F. Hersant, Momentum transport and torque scaling in taylor-couette flow from an analogy with turbulent convection, *The European Physical Journal B - Condensed Matter and Complex Systems* 26 (3) (2002) 379–386. doi:10.1140/epjb/e20020103.
- [22] D. P. Lathrop, J. Fineberg, H. L. Swinney, Transition to shear-driven turbulence in couette-taylor flow, *Physical Review A* 46 (1992) 6390–6405. doi:10.1103/PhysRevA.46.6390.
- [23] T. H. van den Berg, C. R. Doering, D. Lohse, D. P. Lathrop, Smooth and rough boundaries in turbulent taylor-couette flow, *Physical Review E* 68 (2003) 036307. doi:10.1103/PhysRevE.68.036307.
- [24] F. Ravelet, A. Chiffaudel, F. Daviaud, Supercritical transition to turbulence in an inertially driven von krmn closed flow, *Journal of Fluid Mechanics* 601 (2008) 339–364. doi:10.1017/S0022112008000712.